



Transformation of Supercapacitive Charge Storage Behaviour in a Multi elemental Spinel CuMn_2O_4 Nanofibers with Alkaline and Neutral Electrolytes

Ria Kunwar¹ · Syam G. Krishnan² · Izan Izwan Misnon¹ · Fatemeh Zabih³ · Shengyuan Yang³ · Chun-Chen Yang⁴ · Rajan Jose¹

Received: 30 December 2020 / Accepted: 20 April 2021 / Published online: 7 May 2021
© Donghua University, Shanghai, China 2021

Abstract

Electrode material has been cited as one of the most important determining factors in classifying an energy storage system's charge storage mechanism, i.e., as battery-type or supercapacitive-type. In this paper, we show that along with the electrode material, the electrolyte also plays a role in determining the charge storage behaviour of the system. For the purpose of our research, we chose multi-elemental spinel type CuMn_2O_4 metal oxide nanofibers to prove the hypothesis. The material is synthesized as nanofibers of diameter ~ 120 to 150 nm in large scales by a pilot scale electrospinning set up. It was then tested in three different electrolytes (1 M KOH, 1 M Na_2SO_4 and 1 M Li_2SO_4), two of which are neutral and the third is alkaline (KOH). The cyclic voltammograms and the galvanostatic charge–discharge of the electrode material in a three-electrode system measurement showed that it exhibit different charge storage mechanism in different electrolyte solutions. For the neutral electrolytes, a capacitive behaviour was observed whereas a battery-type behaviour was seen for the alkaline electrolyte. This leads us to conclude that the charge storage mechanism, along with the active material, also depends on the electrolyte used.

Keywords Energy storage materials · Electrochemical double layer capacitors · Capacitive charge storage · Ternary manganates · Pseudocapacitors

Introduction

The exponential increase in the usage of portable electronic devices, medical equipment and now, electric vehicles, made the energy storage system (ESS) to be in a much higher demand than ever before; consequently, the ESS industry has come a long way in the last couple of decades [1]. These increase in demands of ESS initiates to explore new energy storage materials with improved efficiency, low cost, and availability. The commercial energy storage device used for these portable electronic gadgets as well as robotic devices are lithium ion batteries (LIB), storing the electrical energy reversibly in it. The ever-increasing cost of lithium, its lower availability and its thermal runaway problem initiated exploring other materials such as zinc, sodium, sulphur, magnesium, and aluminium as energy carriers although the lower cycling stability of the batteries using these carriers hinder their practical deployment [2]. The rise in the electric vehicle markets, owing to the initiation of global CO_2 emission reduction from automobiles by 2030, would require high power devices for its braking as well as automatic door

✉ Rajan Jose
rjose@ump.edu.my

¹ Nanostructured Renewable Materials Research Laboratory, Faculty of Industrial Sciences and Technology, University Malaysia Pahang, 26300 Kuantan, Malaysia

² Graphene & Advanced 2D Materials Research Group (GAMRG), School of Engineering and Technology, Sunway University, No.5 Jalan Universiti, Bandar Sunway, 47500 Petaling Jaya, Selangor, Malaysia

³ State Key Laboratory for Modification of Chemical Fibers and Polymer Materials, International Joint Laboratory for Advanced Fiber and Low-Dimension Materials, College of Materials Science and Engineering, Donghua University, Shanghai, People's Republic of China

⁴ Battery Research Center for Green Energy, Ming Chi University of Technology, New Taipei City, Taiwan

opening applications, thereby requiring higher cycle life of the ESS device.

Supercapacitors, a typical class of energy storage devices, hold its importance in energy storage markets owing to its lower charging and discharging time (power density) and the best reported cycling stability [3]; however with much lower energy density than batteries. Attempts to increase the energy density of supercapacitors are researched through synthesis of various metal oxides, metal chalcogenides, organometallic compounds, ternary metal cobaltites, and various forms of carbons [4]. These materials are electrochemically characterized in a wide range of electrolytes such as aqueous, alkaline, ionic and organic electrolytes for exploring its utility as a supercapacitor material [5, 6]. The charge storage process in supercapacitor is a reversible process in which instantaneous charges will remain the same in charge and discharge processes [7]. Carbons, especially activated carbon (AC), were identified to be supercapacitive material and it store charges in an electric double layer (EDL) between electrode–electrolyte interface [8]. The reversibility of the process was identified from the symmetry of the cyclic voltammetric (CV) studies; redox peaks in CV curves were absent for carbon electrodes in different electrolytes. Similar results were obtained for RuO₂ and MnO₂ as supercapacitor electrodes, the capacitance of these materials was higher than carbons depicting an ion intercalation on a few surface layers, higher than the EDLCs but lower than the batteries [9, 10]. This electrolyte ion intercalation does not change the reversibility of electrodes, hence named as pseudocapacitance (PC) and these materials as pseudocapacitive materials [11, 12]. Based on this categorization, several metal oxides and its composites were tested in alkaline electrolytes and reported as pseudocapacitors [13]. However, the CV curves of these materials possess redox peaks owing to the different redox state of the material and there is asymmetry between charging and discharging curves [14, 15]. Therefore, the instantaneous capacitances of these materials were different at each time interval showing a more battery-type charge storage process and the electrode fabricated using these materials are termed as battery-type electrodes [16, 17].

The argument of battery-type charge storage process as a material property is doubtful. Several factors such as redox states, pore size, surface area, electrolyte ion charge transport parameters including its concentration and solvent, electrode–electrolyte interface resistance, etc., are involved in the charge storage process of a supercapacitor [18, 19]. The electrolyte-ion intercalation changes with the pore size of the material as well as the solvated ion size difference, thereby affecting the amount of charges stored [20]. Furthermore, there are researches reporting on changing the charge storage property of RuO₂ from EDLC to PC with the change in electrolytes [21–23]. Therefore, this paper evaluates the variation of charge storage properties in alkaline and

neutral electrolytes of a random mixed metal spinel oxide (CuMn₂O₄) synthesized as nanowires through electrospinning technique. The variation in the charge storage mode with respect to electrolytes is detailed herewith. The electrochemical characterization of this material as a supercapacitor electrode shows pseudocapacitive behaviour in 1 M Li₂SO₄ and 1 M Na₂SO₄ and battery type charge storage process in 1 M KOH. Therefore, this research paper points out the variation in charge storage process with electrolytes thereby proving that charge storage is not itself an electrode material property; hence, classification of materials or its supercapacitor electrodes as EDLC, PC and battery-type is not appropriate without considering the electrolyte.

Experimental Setup

Synthesis of Material

Metal oxide (CuMn₂O₄) nanofiber compound is synthesized using electrospinning technique. Polymer solution is prepared using 14wt% PVP (avg Mw= 1,30,000 by LS) in 1:1 ratio of DMF and ethanol, stirred overnight in closed container. 3.5 mM of metal-acetate (copper(II)acetate and manganese(II)acetate) precursors (by Sigma Aldrich, USA) are added to the solution prepared above and kept for stirring until a homogeneous solution is obtained (12 h). This heterogeneous solution, with conductivity and viscosity of 144 μ S and 470 cp, is then electrospun (100 needles Bioionica, Fluidnatek, Spain) at a flow rate of 15 mlh⁻¹ with injection and collector voltage fixed at 23 V and – 24 V, respectively. The relative humidity of the apparatus was maintained ~45%, and the temperature was fixed at 50 °C. The electrospun polymer fiber containing the metal precursors are then collected on aluminium foil collector (Fig. 1) and were stored in desiccator for 48 h and peeled off to calcine at 400 °C in a muffle furnace in air at heating rate of 1 °C/min.

The material obtained was characterised using X-ray diffraction (XRD; D2 PHASER, Bruker. Software: DIFFRAC. COMMANDER. Lower discriminator (0.180–0.110 V), Upper discriminator (0.250–0.5 V), 2Theta (10–80)), Scanning Electron Microscopy (SEM; Hitachi S-2600H, Japan) and Field Emission Scanning Emission Microscopy (FESEM, JSM-7800F, JEOL, Japan).

Electrochemical Analysis

For electrochemical energy storage investigation, the electrodes were fabricated by coating slurry of the active material on pre-cleaned nickel foam substrates using acetone, HCl, water, and ethanol. The slurry, for the purpose of this experiment, was prepared by mixing the active material with polyvinylidene fluoride (PVDF) (Sigma Aldrich, USA) and

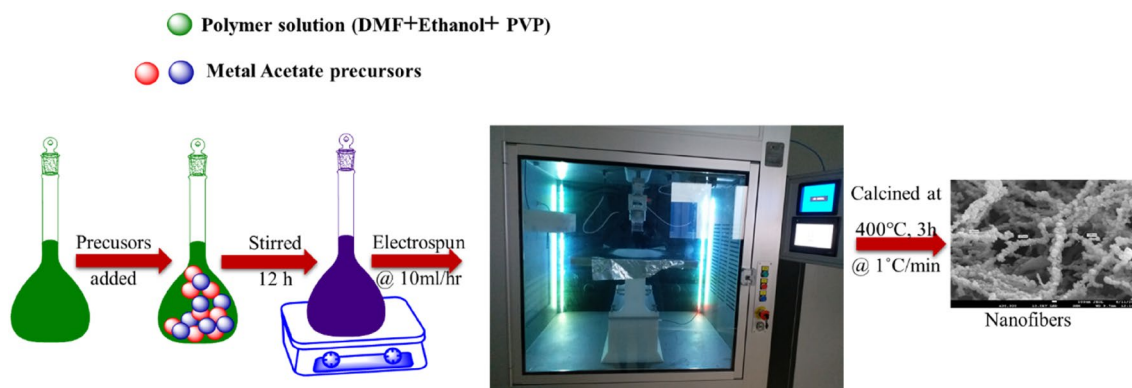


Fig. 1 Schematic of experimental setup for nanofiber preparation

carbon black (Super P conductive, Alfa Aesar, UK) in the ratio 80:10:10. N-methyl-2-pyrrolidinone (NMP), which works as a homogenizer, was added to the above mixture and stirred well for 24 h. The prepared slurry was pasted on an area of 1 cm^2 over the pre-cleaned nickel substrate and dried overnight at 65°C . After drying the electrodes are pressed using a hydraulic press with pressure of 5 tonnes to ensure the homogeneity of the material in the electrode surface. The active material loading on the electrodes was determined to be $\sim 2.2 \text{ mg cm}^{-2}$ for all the electrodes.

The cyclic voltammetry (CV), charge–discharge cycles (CDC) and electrochemical impedance spectroscopy (EIS) measurements of the electrodes were studied using potentiostat–galvanostat (PGSTAT M101, Metrohm Autolab B.V., Netherlands) employing NOVA 1.9 software. The EIS measurements were recorded in the frequency range of $100 \text{ kHz}–0.01 \text{ Hz}$ at the respective open circuit potential. The electrochemical characterizations were performed using $1 \text{ M Na}_2\text{SO}_4$, 1 M KOH and $1 \text{ M Li}_2\text{SO}_4$ in a three-electrode configuration using working electrode, Ag/AgCl as reference electrode and a platinum wire as the counter electrode.

Result and Discussions

Structure and Morphology

The crystal structure of the material is analysed through XRD; the XRD pattern of the CuMn_2O_4 nanofibers refined by the Rietveld method using the TOPAS software is shown in Fig. 2. The pattern shows cubic spinel structure of the material through peaks corresponding to (111), (022), (311), (222), (004), (331), (422), (333), (044), (442), (062), (533) and (622) crystal planes at $2\theta \sim 19^\circ, \sim 30^\circ, \sim 36^\circ, \sim 38^\circ, \sim 44^\circ, \sim 48^\circ, \sim 54^\circ, \sim 58^\circ, \sim 63^\circ, \sim 68^\circ, \sim 72^\circ, \sim 75^\circ, \text{ and } \sim 76^\circ$ respectively. The Goodness-of-Fit indicator $S = 1.27$, which is defined as $S = R_{\text{wp}}/R_{\text{p}}$, is

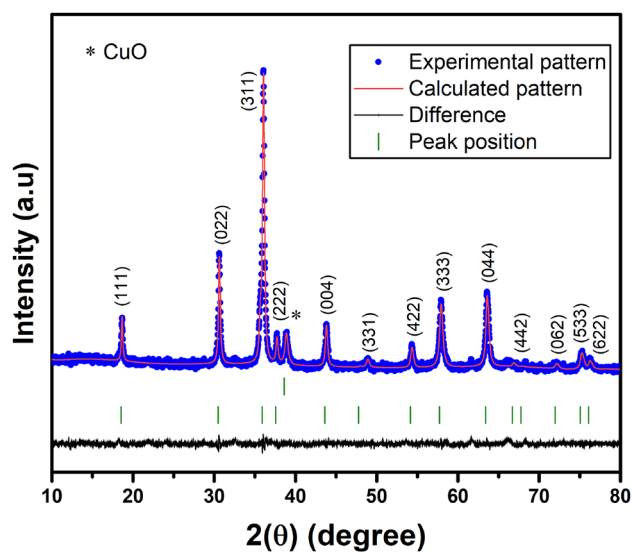


Fig. 2 Rietveld refinement plot of CuMn_2O_4 . The solid circles are the experimental pattern, the continuous lines are the calculated pattern. The bottom continuous line gives the difference between the calculated and the experimental pattern. The bottom vertical lines are the Bragg reflection positions of the standard spinel structure of the CuMn_2O_4 for $\lambda = 1.5406 \text{ \AA}$ radiation. The middle vertical line corresponds to the CuO peak marked in *

within the optimum range of 1.2–1.4, from which it can be concluded that the fitting between the calculated and the observed diffraction profiles are in good agreement. The volume of unit cell calculated from the pattern is 569.87 \AA^3 . A secondary phase peak corresponding to CuO has been detected and identified by (*) in the plot; however, the fraction of CuO in the mixture is considerably lower ($\sim 2\%$), which is not expected to influence the electrochemical properties in a significant way. The residues of fitting (R_{p} , R_{wp} and R_{exp}) as well as physical parameters such as lattice parameter, lattice volume, crystallite size, lattice

strain, linear absorption coefficient, density of the unit cell, obtained from the refinement are listed in Table 1.

The morphology of the sample analysed using FESEM is in Fig. 3. Images of different resolution were recorded, a fibre-like morphology was observed for the sample. The fibres consisted of agglomeration of nanoparticles and the fibre thickness was measured to be ~ 120–150 nm.

Table 1 Reitveld refinement parameters

Parameter	Values
Space group	Fd $\bar{3}m$
a (Å)	8.2907
Cell Volume (Å ³)	569.87
R-Bragg	0.141
R _p (%)	1.66
R _{wp} (%)	2.10
R _{exp} (%)	1.83
S (=R _{wp} /R _p)	1.27
Wt%—Rietveld	100.0
Crystallite Size Lorentzian (nm)	66.4
Lattice Strain	0.2373
Crystal Linear Absorption Coeff. (cm ⁻¹)	3721.86

Electrochemical Properties

Cyclic Voltammetry (CV)

The cyclic voltammograms of the material in different electrolytes are shown in Fig. 4a–c. The reversibility of the electrodes to be evaluated from the symmetry of the CV curves determines the charge storage process in them. A highly symmetric CV curve without any clear redox peaks is indicative of similar charge assembly at regular voltage intervals, thereby demonstrating pure EDLC; whereas small deviation from symmetry still without any redox peaks characterizes pseudocapacitive properties [14, 16, 19]. On the other hand, clear oxidation and reduction peaks occurring at different potentials are indicative of battery-type storage process [14, 16, 19]. In the 1 M KOH electrolyte, the CV curves of the electrodes in Fig. 4a show (i) clear redox peaks and (ii) varying instantaneous charges in different voltage intervals, thereby showing battery type charge storage process as has been recommended previously [14, 16, 19]. Previous researchers show that the oxidation/reduction process in the CuMn₂O₄ electrode can be understood from the reaction schemes shown in (1).

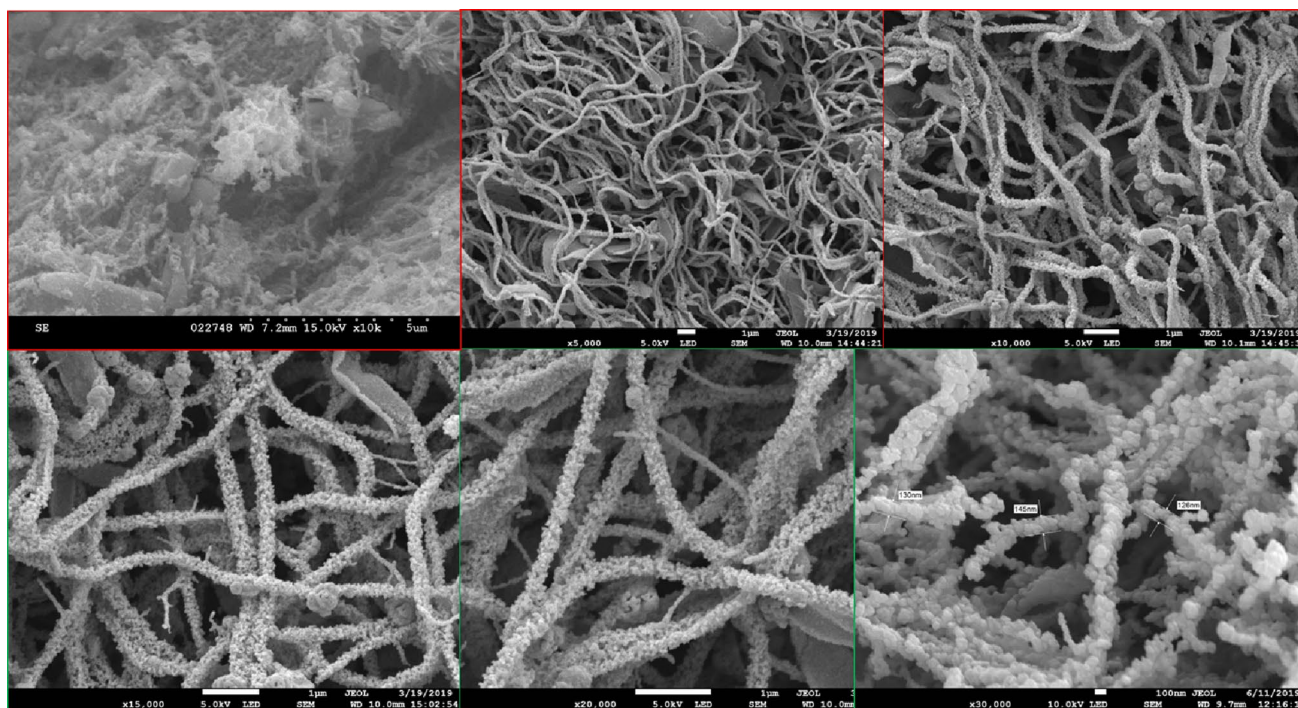


Fig. 3 The FESEM images of the CuMn₂O₄ at various magnifications

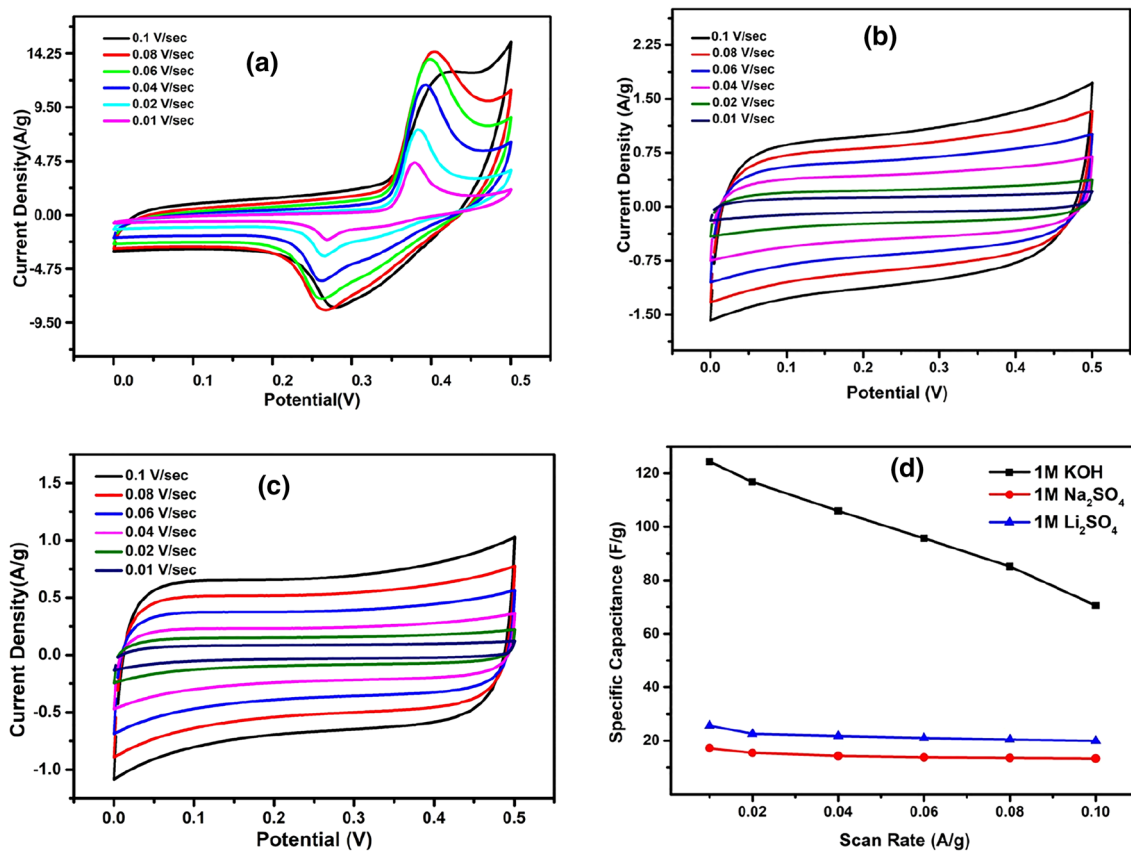
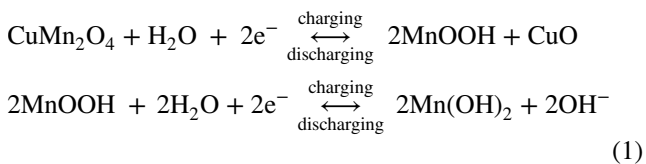


Fig. 4 CV curves of CuMn₂O₄ nanofiber in **a** 1 M KOH, **b** 1 M Li₂SO₄, **c** 1 M Na₂SO₄, at different scan rates (d) Comparison of variation in specific capacitance in different electrolytes at different scan rates



i.e., in 1 M KOH, the redox peaks in the CV curves of the CuMn₂O₄ can be explained as the transformation of Mn³⁺/Mn⁴⁺ [24–26] and Cu²⁺/Cu transformation [27, 28]. However, the redox peaks formed in 1 M KOH electrolyte show low symmetry curves and clear redox processes compared to other two neutral electrolytes (1 M Li₂SO₄ and 1 M Na₂SO₄). As understood from the literature, the conductivity as well as solvated ion size of these neutral electrolytes were inferior compared to alkaline electrolytes [29, 30]. Usually, neutral electrolytes possess potential window in the range of ~1 to 2 V [31, 32]. However, since this study compares the charge-storage property of the electrode–electrolyte interface rather than electrode property, the potential window (V) of the electrochemical studies in these series of experiments was fixed at 0.5 V for all the electrolytes. The hydrated ion size of Li⁺ (38.2 nm)

and Na⁺ (35.8 nm) is higher than K⁺ (33.1 nm) [32]. Further, K⁺ ions also have an improved ionic conductivity compared to the Li⁺ and Na⁺ ions. Therefore, the improved conductivity of KOH electrolyte could have resulted in deeper solvated ion intercalation to the electrode surface compared to the other two. This deeper ion intercalation to the electrode surface could have lowered reversibility of charge-storage process showing prominent charge–discharge process. Further observing the redox peaks of the CV curves in KOH electrolyte at higher rates, the redox peaks changes its position in positive and negative region showing the variation of charge storability at different scan rates. The larger solvated ion size of Li₂SO₄ and Na₂SO₄ would have denied its deeper ion intercalation compared to KOH. Therefore, the charge storage property of the same material (CuMn₂O₄) is varied; more of a battery-type in KOH electrolyte and supercapacitive in Li₂SO₄ and Na₂SO₄ electrolyte. Therefore, categorising electrode materials as supercapacitive and battery-type material is questionable.

The capacitance from the CV curves for these materials could be calculated using the Eq. (2)

$$C_s = \frac{1}{m \times \text{ScanRate} \times \text{PotentialWindow}} \int CV\text{curve} \quad (2)$$

The capacitance of CuMn_2O_4 was superior in KOH electrolyte ($\sim 124 \text{ F.g}^{-1}$) compared to Li_2SO_4 ($\sim 26 \text{ F.g}^{-1}$), and Na_2SO_4 ($\sim 17 \text{ F.g}^{-1}$) at a scan rate of 10 mV s^{-1} . The higher capacitance of CuMn_2O_4 in KOH electrolyte shows improved electrode–electrolyte interaction owing to the improved ionic conductivity of electrolyte, and the one-dimensional pathways offered by the materials. Figure 4d compares the variation of capacitance of CuMn_2O_4 with increase in scan rate. The plot shows that there is $\sim 57\%$ of capacitance retention with 10 times increase in scan rate whereas the retention was $\sim 77\%$ and $\sim 78\%$, in Na_2SO_4 and Li_2SO_4 , respectively. The C_s obtained by CuMn_2O_4 in all the three electrolytes were lower compared to the other materials reported by our group earlier [33–35]. However, the scope of this paper is not on the energy storage capacity of the material but on understanding the charge storage process as an electrode–electrolyte system than categorising it as a battery-type or supercapacitor material.

Galvanostatic Charge Discharge (GCD)

The practical charge storage capacity of the electrode is calculated using charge–discharge cycling. The difference in charge storage process with the variation of electrolyte could be determined by the shape of GCD curves in Fig. 5. Figure 5a show the GCD curve of CuMn_2O_4 in 1 M KOH. There is a clear asymmetry between charge and discharge cycles showing battery-type charge storage and the two charge–discharge plateaus between 0.35 and 0.5 V, increasing its charging as well as discharging time. It could be observed that the maximum capacitance of the material is obtained in this voltage range and the capacitance drastically decreases after this voltage range. Similar charge–discharge behaviour was observed for transition metal oxide nanofibers such as Co_3O_4 [36], CuO [27], and NiO [4] in KOH electrolyte. Therefore, this battery-type charge property of CuMn_2O_4 could be attributed to the solvated ion intercalation of KOH to the electrode surface. This intercalation increases the redox reaction of $\text{Mn}^{3+}/\text{Mn}^{4+}$ and Cu^{2+}/Cu process compared to the other two neutral electrolytes.

The GCD curves of CuMn_2O_4 (Fig. 5b, c) show almost similar charge–discharge curves without any

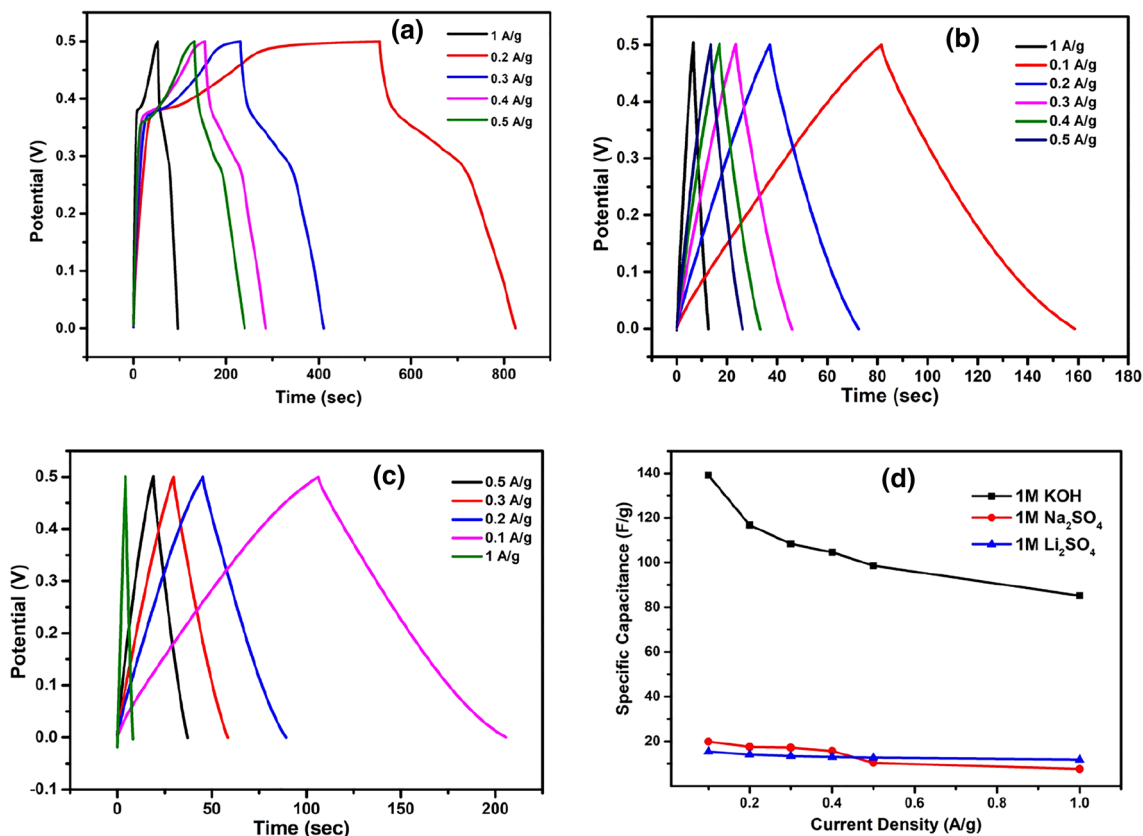


Fig. 5 GCD curves of CuMn_2O_4 nanofiber in **a** 1 M KOH, **b** 1 M Li_2SO_4 , and **c** 1 M Na_2SO_4 , and **d** Comparison of variation in specific capacitance in different electrolytes at different scan rates

charge–discharge plateau. The coulombic efficiency (η) of the electrode is defined as the ratio of discharging to charging time and determined to be 91.62%, 90.62%, and 88.79 at 1A/g for KOH, Li_2SO_4 , and Na_2SO_4 electrolytes, respectively. The result shows a comparable η for neutral electrolytes compared to KOH electrolyte. This smooth charge–discharge process is also desirable for a power device electrode such as supercapacitor. The resistance of the electrode (R_s) to the ion intercalation could be calculated from the ratio of potential drop to the change in current. The R_s value of the electrodes were determined to be 1.85 Ω , 6.25 Ω , and 6.20 Ω , at 1A/g for KOH, Li_2SO_4 , and Na_2SO_4 , respectively. The difference in the resistance of the electrode depends on the ionic conductivity of the electrolyte as well as its solvated ion size. Therefore, the R_s value of the electrode to KOH ion intercalation was lower thereby proving its asymmetric behaviour.

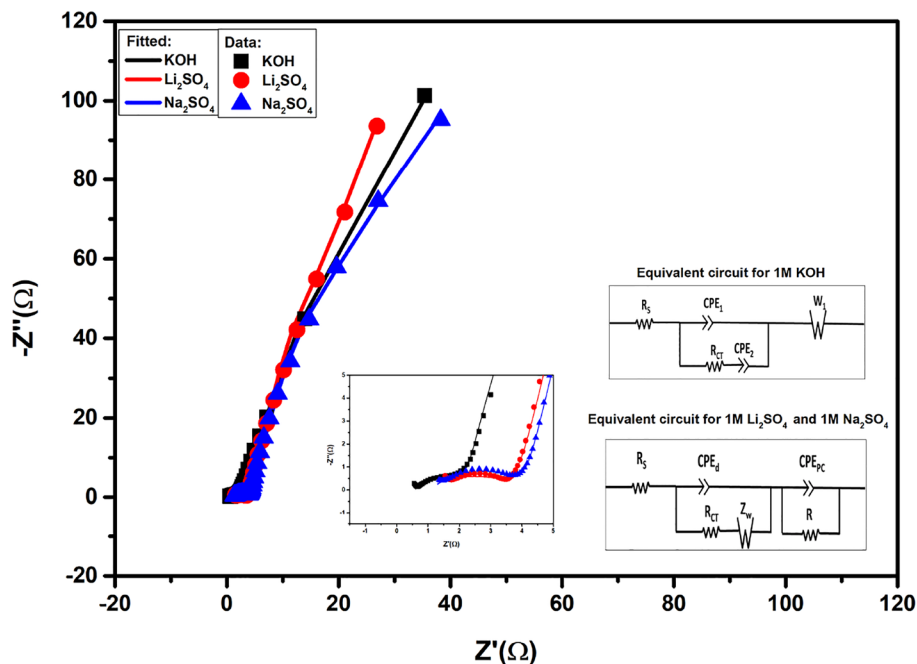
The capacitance decreases with increase in current density for the electrode in all the electrolytes (Fig. 5d). Similar to the capacitance reduction with increase in scan rate from CV curves, the C_s reduced to ~ 60%, ~ 78%, and ~ 58%, for KOH, Li_2SO_4 , and Na_2SO_4 respectively. It could be observed from Fig. 5a that the asymmetry in CD curves reduced with increased current density showing a decrease in faradic reaction at higher current densities. The C_s retention was higher for Li_2SO_4 electrolyte validating its capacitance retention from CV curves. The charge storage property variation with alkaline and neutral electrolyte create doubt on categorising the material as battery-type and pseudocapacitive material.

Electrochemical Impedance Spectroscopy (EIS)

The electrochemical impedance spectroscopy (EIS) study determines the electrode–electrolyte interaction as well as the electrode resistance. It was performed in the frequency range of 0.1 MHz to 2 MHz with an ac variation of 10 mV. The Nyquist plot of CuMn_2O_4 in 1 M KOH, 1 M Li_2SO_4 , and 1 M Na_2SO_4 could describe three processes (a) the resistive effects such as electrode series resistance (ESR) or the electrode resistance (R_s) at higher frequencies (> 1 kHz), (b) intermediate frequencies (< 1 kHz) determine the capacitive effects, and (c) the lower frequencies (< 5 Hz) determining Warburg impedance due to electrolyte–electrode ion diffusion process. The R_s value combines the electrolytic, electrode and contact resistance at the interface due to ionic diffusion. As expected, due to higher ionic conductivity of KOH electrolyte, the R_s value of CuMn_2O_4 is lower (0.64 Ω); and the electrode resistances were comparatively higher in the neutral electrolytes (Li_2SO_4 and Na_2SO_4), determined to be 1.35 Ω , and 1.26 Ω , respectively.

The inset of the Nyquist plot shows the transformation of charge behaviour from higher to lower frequencies. The diameter of the small semicircle present in the EIS spectrum of CuMn_2O_4 for all the three electrodes show the charge transfer resistance (R_{CT}). R_{CT} measures the resistance offered by the CuMn_2O_4 -electrolyte interface to the diffusion of electrolyte ions and is determined to be 1.12 Ω , 2.375 Ω , and 2.759 Ω , in 1 M KOH, 1 M Li_2SO_4 , and 1 M Na_2SO_4 , respectively. The straight line after the same circle shows the intermediate frequency region of the Nyquist plot and if the curve is more inclined towards the imaginary y-axis, it

Fig. 6 EIS measurement of CuMn_2O_4 nanofiber in 1 M KOH, 1 M Li_2SO_4 and 1 M Na_2SO_4 , and its respective equivalent circuit deployed for fitting



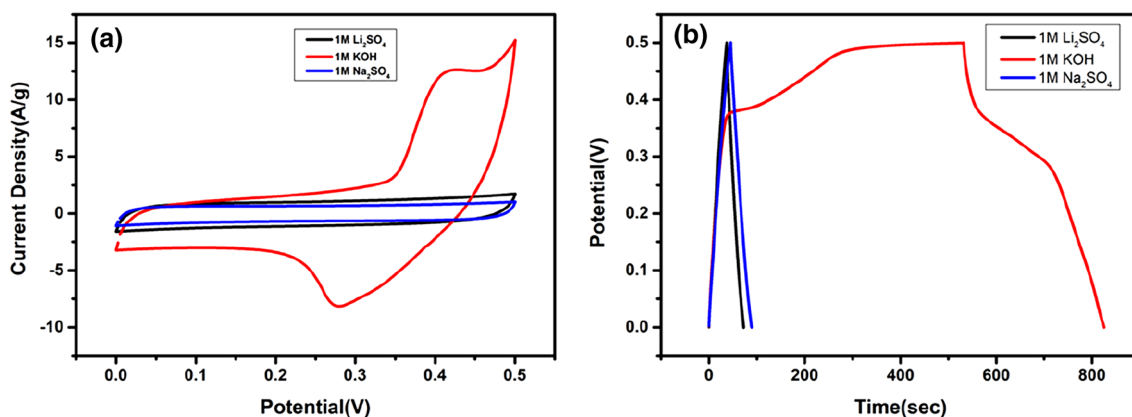


Fig. 7 **a** CV comparison for 1 M KOH, 1 M Na₂SO₄ and 1 M Li₂SO₄ at scan rate of 0.1 V/s; **b** GCD comparison of 1 M KOH, 1 M Na₂SO₄ and 1 M Li₂SO₄ at current density of 0.2 A/g

shows EDLC property or lower ion diffusion between electrode–electrolyte surface. From the inset of Fig. 6, it can be determined that the inclination is more towards the real axis (x-axis) compared to the insets in Fig. 6. The change in charge-transport behaviour of the electrode towards different electrolyte system could be observed; for KOH the charge storage consists of more ion diffusion process, whereas in Li₂SO₄ and Na₂SO₄, the double layer formation dominates the charge storage. Therefore, these two characteristic resistances from the Nyquist plot show variation in charge storage behaviour in CuMn₂O₄ electrode. The intermediate frequency region of the Nyquist plot justifies the CV analysis of involving diffusion process in charge storage process (Fig. 7a). This ion diffusion increased the Faradic reaction thereby increasing the redox process thereby showing redox peaks. The double layer charge storage process with Li₂SO₄ and Na₂SO₄ electrolytes for CuMn₂O₄ electrode is similar to the charge storage process in carbon electrodes [12] thereby validating our views on electrode–electrolyte system than an electrode material. Similarly, Fig. 7b show that KOH electrolyte improved the charge storage process as the plateau from 0.35 to 0.5 V demonstrate the diffusion process at the intermediate frequencies as determined from EIS. Figure 6 also consist of equivalent circuit of the charge storage process showing the difference in charge storage process of CuMn₂O₄ with electrolyte.

Conclusions

A ternary spinel cobaltite (CuMn₂O₄) nanowire is electrochemically analysed for the determination of variation in charge storage process. It was determined that KOH electrolyte-initiated diffusion-controlled charge storage process where as Li₂SO₄ and Na₂SO₄ electrolytes stored charges in electric double layer process. A maximum C_s of ~ 123 F g⁻¹

@ 0.1 A g⁻¹ was obtained for the material in 1 M KOH electrolyte. The transformation of charge storage process from diffusion-controlled process involving faradic reaction as well as redox peaks to a double layer charge formation proves that charge storage is not only a material property. Thus, it is shown that the charge storage property of the material could change with the choice of electrolytes.

Acknowledgements This work is funded by the Fundamental Research Grant Scheme of the Ministry of Education, Govt. of Malaysia through FRGS/1/2019/STG07/UMP/01/1 (<http://www.ump.edu.my>). Ria expresses gratitude to Battery Research Centre of Green Energy (BRCGE) of Ming Chi University of Technology, New Taipei, Taiwan and Taiwan Experience Education Program (TEEP@AsiaPlus) for their research financial support.

Declarations

Conflicts of interest The authors have no conflicts to declare.

References

1. Tebyetekerwa M, Marriam I, Xu Z, Yang S, Zhang H, Zabihi F, Jose R, Peng S, Zhu M, Ramakrishna S. Critical insight: challenges and requirements of fibre electrodes for wearable electrochemical energy storage. *Energy Environ Sci*. **2019**;12(7):2148–60.
2. Pal B, Yang S, Ramesh S, Thangadurai V, Jose R. Electrolyte selection for supercapacitive devices: a critical review. *Nanos Adv*. **2019**;1(10):3807–35.
3. Conway BE. Electrochemical supercapacitors: scientific fundamentals and technological applications. Berlin: Springer Science & Business Media; **2013**.
4. Kunwar R, Harilal M, Krishnan SG, Pal B, Misnon II, Mariappan CR, Ezema FI, Elim HI, Yang CC, Jose R. Pseudocapacitive Charge Storage in Thin Nanobelts. *Adv Fiber Mater*. **2019**;1(3):205–13.
5. Singh A, Chandra A. Significant performance enhancement in asymmetric supercapacitors based on metal oxides, carbon nanotubes and neutral aqueous electrolyte. *Sci Rep*. **2015**;5:15551.

6. Galiński M, Lewandowski A, Stepniak I. Ionic liquids as electrolytes. *Electrochim Acta*. **2006**;51(26):5567–80.
7. Jiang W, Hu F, Yan Q, Wu X. Investigation on electrochemical behaviors of NiCo₂O₄ battery-type supercapacitor electrodes: the role of an aqueous electrolyte. *Inorg Chem Front*. **2017**;4(10):1642–8.
8. Kang J, Wen J, Jayaram SH, Yu A, Wang X. Development of an equivalent circuit model for electrochemical double layer capacitors (EDLCs) with distinct electrolytes. *Electrochim Acta*. **2014**;115:587–98.
9. Abd Aziz R, Jose R. Charge storage capability of tunnel MnO₂ and alkaline layered Na-MnO₂ as anode material for aqueous asymmetry supercapacitor. *J Electroanal Chem*. **2017**;799:538–46.
10. Krishnan SG, Harilal M, Pal B, Misnon II, Karuppiyah C, Yang CC, Jose R. Improving the symmetry of asymmetric supercapacitors using battery-type positive electrodes and activated carbon negative electrodes by mass and charge balance. *J Electroanal Chem*. **2017**;805:126–32.
11. Jiang Y, Liu J. Definitions of pseudocapacitive materials: a brief review. *Energy Environ Mater*. **2019**;2(1):30–7.
12. Misnon II, Zain NKM, Lei TS, Vijayan BL, Jose R. Activated carbon with graphitic content from stinky bean seedpod biowaste as supercapacitive electrode material. *Ionics*. **2020**;26(8):4081–93.
13. Augustyn V, Simon P, Dunn B. Pseudocapacitive oxide materials for high-rate electrochemical energy storage. *Energy Environ Sci*. **2014**;7(5):1597–614.
14. Brousse T, Bélanger D, Long JW. To be or not to be pseudocapacitive. *J Electrochem Soc*. **2015**;162(5):A5185–9.
15. Sun J, Wu C, Sun X, Hu H, Zhi C, Hou L, Yuan C. Recent progresses in high-energy-density all pseudocapacitive-electrode-materials-based asymmetric supercapacitors. *J Mater Chem A*. **2017**;5(20):9443–64.
16. Brousse T, Long JW, Bélanger D. Pseudocapacitive vs battery type electrodes: two distinctive aspects of fast electrochemical processes and devices In: 232nd ECS Meeting (October 1–5, 2017), 2017.
17. Dubal DP, Ayyad O, Ruiz V, Gomez-Romero P. Hybrid energy storage: the merging of battery and supercapacitor chemistries. *Chem Soc Rev*. **2015**;44(7):1777–90.
18. Harilal M, Krishnan SG, Yar A, Misnon II, Reddy MV, Yusoff MM, Ojur Dennis J, Jose R. Pseudocapacitive charge storage in single-step-synthesized CoO–MnO₂–MnCo₂O₄ hybrid nanowires in aqueous alkaline electrolytes. *J Phys Chem C*. **2017**;121(39):21171–83.
19. Gogotsi Y, Penner RM. Energy storage in nanomaterials—capacitive, pseudocapacitive, or battery-like? *ACS Nano*. **2018**;12(3):2081–3.
20. Lewandowski A, Olejniczak A, Galinski M, Stepniak I. Performance of carbon–carbon supercapacitors based on organic, aqueous and ionic liquid electrolytes. *J Power Sources*. **2010**;195(17):5814–9.
21. Béguin F, Presser V, Balducci A, Frackowiak E. Carbons and electrolytes for advanced supercapacitors. *Adv Mater*. **2014**;26(14):2219–51.
22. Krishnan SG, Arulraj A, Khalid M, Reddy MV, Jose R. Energy storage in metal cobaltite electrodes: Opportunities & challenges in magnesium cobalt oxide. *Renew Sustain Energy Rev*. **2021**;141:110798.
23. Vijayan BL, Misnon II, Karuppiyah C, Kumar GM, Yang S, Yang S, Jose R. Thin metal film on porous carbon as a medium for electrochemical energy storage. *J Power Sources*. **2021**;489:229522.
24. Li Z-Y, Akhtar MS, Bui PTM, Yang OB. Predominance of two dimensional (2D) Mn₂O₃ nanowalls thin film for high performance electrochemical supercapacitors. *Chem Eng J*. **2017**;330:1240–7.
25. Wang X, Liu L, Wang X, Yi L, Hu C, Zhang X. Mn₂O₃/carbon aerogel microbead composites synthesized by in situ coating method for supercapacitors. *Mater Sci Eng B*. **2011**;176(15):1232–8.
26. Zhang LL, Wei T, Wang W, Zhao XS. Manganese oxide–carbon composite as supercapacitor electrode materials. *Microporous Mesoporous Mater*. **2009**;123(1–3):260–7.
27. Vidhyadharan B, Misnon II, Abd Aziz R, Padmasree KP, Yusoff MM, Jose R. Superior supercapacitive performance in electrospun copper oxide nanowire electrodes. *J Mater Chem A*. **2014**;2(18):6578–88.
28. Harilal M, Krishnan SG, Pal B, Reddy MV, Ab Rahim MH, Yusoff MM, Jose R. Environment-modulated crystallization of Cu₂O and CuO nanowires by electrospinning and their charge storage properties. *Langmuir*. **2018**;34(5):1873–82.
29. Paul S, Choi KS, Lee DJ, Sudhagar P, Kang YS. Factors affecting the performance of supercapacitors assembled with polypyrrole/multi-walled carbon nanotube composite electrodes. *Electrochim Acta*. **2012**;78:649–55.
30. Salunkhe RR, Kaneti YV, Yamauchi Y. Metal–organic framework-derived nanoporous metal oxides toward supercapacitor applications: progress and prospects. *ACS Nano*. **2017**;11(6):5293–308.
31. Wu Y-Z, Ding Y, Hayat T, Alsaedi A, Dai SY. Enlarged working potential window for MnO₂ supercapacitors with neutral aqueous electrolytes. *Appl Surf Sci*. **2018**;459:430–7.
32. Zhong C, Deng Y, Hu W, Qiao J, Zhang L, Zhang J. A review of electrolyte materials and compositions for electrochemical supercapacitors. *Chem Soc Rev*. **2015**;44(21):7484–539.
33. Vijayan BL, Krishnan SG, Nk Z, Harilal M, Yar A, Misnon II, Dennis OJ, Yusoff MM, Jose R. Large scale synthesis of binary composite nanowires in the Mn₂O₃–SnO₂ system with improved charge storage capabilities. *Chem Eng J*. **2017**;327:962–72.
34. Pal B, Vijayan BL, Krishnan SG, Harilal M, Basirun WJ, Lowe AA, Yusoff MM, Jose R. Hydrothermal syntheses of tungsten doped TiO₂ and TiO₂/WO₃ composite using metal oxide precursors for charge storage applications. *J Alloys Compd*. **2018**;740:703–10.
35. Vijayan BL, Misnon II, Kumar GM, Miyajima K, Reddy MV, Zaghbi K, Karuppiyah C, Yang CC, Jose R. Facile fabrication of thin metal oxide films on porous carbon for high density charge storage. *J Colloid Interface Sci*. **2020**;562:567–77.
36. Anuradha CT, Raji P. Facile synthesis and characterization of Co₃O₄ nanoparticles for high-performance supercapacitors using *Camellia sinensis*. *Appl Phys A*. **2020**;126(3):164.



Ria Kunwar is a doctoral student at the Nanostructured Renewable Energy Material Laboratory (NREML), Faculty of Industrial Sciences and Technology, Universiti Malaysia Pahang. Working under the supervision of Prof. Jose Rajan and Dr. Izan Izwan Misnon, her current research interest includes synthesis of novel energy storage materials and electrical modelling of supercapacitors and battery behaviors.



Syam G. Krishnan received his Ph.D. in Physics from the Faculty of Industrial Sciences and Technology, Universiti Malaysia Pahang under the supervision of Prof. Jose Rajan. Currently, he is working as a research fellow in Graphene and Advanced 2D Materials Research Group (GAMRG), School of Engineering and Technology, Sunway University, Malaysia. His research interests are focused on developing new energy storage materials for supercapacitors and lithium-ion batteries. He also

researches tailoring the porosity and surface area of activated carbons produced from biowastes.

focused on low-dimensional, Fiber Shaped and solar-driven multifunctional devices.



Shengyuan Yang is an associate Professor in the College of Materials Science and Engineering, Donghua University. He obtained his Ph.D from National University of Singapore sponsored by the prestigious NGS Scholarship. His research is centered around novel applications of electrospun nanofibers towards smart wearables. He also leads the DHU International Cooperation Office.



Izan Izwan Misnon is a Senior Lecturer at the Faculty of Industrial Sciences and Technology, Universiti Malaysia Pahang, from where he received his doctoral degree in 2016. He is working on electrodes for electrochemical capacitors, batteries; electrospun membranes, sensors, carbon and cellulosic material functionalization; and waste-to-wealth screening of indigenous biomass.



Chun-Chen Yang is a Professor of Chemical Engineering and the Director of Battery Research Center of Green Energy at the Ming Chi University of Technology, Taiwan. His major research efforts focus are on alkaline DMFC, PEMFC, Polymer electrolyte membranes, Zn-air battery, Ni-MH battery, and Li-ion batteries, and supercapacitors.



Fatemeh Zabih is a senior researcher and faculty member at the State Key Laboratory for Modification of Chemical Fibers and Polymer Materials, College of Material Science and Engineering of Donghua University, Shanghai, China. She received her PhD from IAU, Tehran Science and Research Branch. She previously worked as a post-doctoral fellow and senior researcher in the University of Michigan – Shanghai Jiao Tong University Joint Institute in the School of Chemistry and Chemical

Engineering from 2012 to 2016. Her current research is mainly



Rajan Jose is a Professor in the Faculty of Industrial Sciences & Technology, Universiti Malaysia Pahang and supervises the Nanostructured Renewable Energy Materials Laboratory. His current research interests include circular economy, data science, renewable materials and devices; most of his research is on the structure – property relationship in materials for a desired device functionality.